ELSEVIER

Chemical Geology 237 (2007) 450–465

CHEMICAL GEOLOGY
INCLUDING
ISOTOPE GEOSCIENCE

www.elsevier.com/locate/chemgeo

Microstructures and composition of melt inclusions in a crustal anatectic environment, represented by metapelitic enclaves within El Hoyazo dacites, SE Spain

Antonio Acosta-Vigil [a,*], Bernardo Cesare [a,b], David London [c], George B. Morgan VI [c]

[a] *Istituto di Geoscienze e Georisorse, Consiglio Nazionale delle Ricerche, Padova, Italy*
[b] *Dipartimento di Mineralogia e Petrologia, Università di Padova, Padova, Italy*
[c] *School of Geology and Geophysics, University of Oklahoma, Norman OK, USA*

Accepted 10 July 2006

Editor: R. Rudnick

Abstract

This article reports microstructures and compositions of melt inclusions in anatectic metapelites found as enclaves within El Hoyazo dacites, in the Neogene Volcanic Province of southeastern Spain. The enclaves represent fragments of continental crust partially melted at ~800–850 °C and 5–7 kbar, and brought to surface rapidly within the host volcanics while they still were in a molten state. Rapid cooling produced the solidification of silicate melt to glass in the rock matrix and in inclusions within minerals. Melt inclusions (MI) are present within nearly all mineral phases in the enclaves, and their associated microstructures indicate a primary or pseudo-secondary origin. The entrapment mechanisms of MI within plagioclase were associated with: (1) the presence of micron-sized solids (mostly graphite) on the surface of growing crystals; (2) partial resorption of crystals, generation of embayments, and later growth in the presence of melt; and (3) entrapment of melt during crystal growth within crystallographic-controlled planar structures, e.g. on crystal faces. Melt inclusions in garnet are commonly associated with regularly oriented planar discontinuities filled with glass, interpreted either as spaces left between adjacent mineral growth spirals or as crystallographic-controlled cracks generated in-between stages of mineral growth. Melt was trapped or percolated along these microstructures and, later on, necking down phenomena individualized inclusions with negative crystal shape. Melt inclusions in biotite are abundant, show negative crystal shape, and parallel cleavage planes. Melt inclusions in cordierite, alkali feldspar and ilmenite are isolated, sparse and sometimes rather large. The composition of glass from all MI is leucogranitic and peraluminous, with small differences among glasses in each mineral host. There is some variation in glass composition within each textural location as well. Compositional heterogeneity can be partially explained by a combination of processes such as generation of boundary layers during mineral growth, crystallization of daughter phases, and hydrogen loss via diffusion through the host. Mean glass compositions in the several textural locations, however, can be tentatively interpreted as reflecting the evolution of melt chemistry during the prograde low-to-medium pressure anatexis of quartz-poor metapelites.

Keywords: Metasedimentary enclaves; Crustal anatexis; Melt inclusions; Fluid inclusions

1. Introduction

The study of inclusions of fluid (FI) and silicate glass (MI) within minerals can provide valuable information on the composition, chemical evolution, and role of

* Corresponding author. Present address: Departamento de Mineralogía y Petrología, Facultad de Ciencias, Universidad de Granada, Campus Fuentenueva s/n, 18002 Granada, Spain. Tel.: +34 958 248535; fax: +34 958 243368.
E-mail address: aacosta@ugr.es (A. Acosta-Vigil).

0009-2541/$ - see front matter © 2006 Elsevier B.V. All rights reserved.
doi:10.1016/j.chemgeo.2006.07.014

fluids and melts during geologic processes (e.g. Roedder, 1984; Frezzotti, 2001). Most studies of MI associated with crustal environments have dealt with the relatively late evolutionary stages of magmatic systems, such as allocthonous granites (e.g. Thomas and Klemm, 1997; Webster et al., 1997; Audétat et al., 2000) and volcanics (e.g. Webster and Duffield, 1991; Lu et al., 1992; Peppard et al., 2001). Studies of MI in crustal anatectic environments are very scarce, related in part to the difficulty of finding or recognizing former MI in anatectic rocks due to post-entrapment modifications taking place upon slow cooling (e.g. Frezzotti, 2001). Accurate information on the composition of melt during crustal anatexis in natural environments comes mostly from the analysis of glasses in anatectic enclaves found within volcanics (e.g. Grapes, 1986; Cesare et al., 1997; Braun and Kriegsman, 2001; Cesare et al., 2003a,b; Frezzotti et al., 2004; Zanon and Nikogosian, 2004; Salvioli-Mariani et al., 2005). The rapid ascent and extrusion of the enclaves within the host magma results in quenching of melt to glass, with preservation of mineral and melt compositions and textural relationships during anatexis. Hence, the study of enclaves has also the potential of providing information on the mechanisms of crustal melting in nature. This information can be gained through the combination of detailed geochemical and microstructural analyses of enclaves, and comparison with available experimental data on both the equilibrium partial melting and the kinetics of melting of crustal protoliths (Grapes, 1986; Frezzotti et al., 2004; Acosta-Vigil et al., 2006a).

During the last decade Cesare and coworkers have studied the petrology of anatectic metapelitic enclaves within volcanics of the Neogene Volcanic Province (NVP) of southeastern Spain (Cesare et al., 1997, 2003a; Alvarez-Valero et al., 2005; and references therein). These rocks are a unique natural laboratory for the study of crustal melting, as they contain the first known examples in the world where preserved MI are hosted within minerals such as cordierite, andalusite, hercynite, ilmenite, zircon and monazite. Cesare et al. (1997, 2003b) and Cesare and Gómez-Pugnaire (2001) have conducted a reconnaissance study of the composition of glasses within enclaves, showing the existence of some heterogeneity within and among the several textural locations. Present paper represents the first extensive study of microstructures and chemistry of MI in enclaves of the NVP volcanics. It consists of a detailed petrographic, scanning electron microscope (SEM) and electron microprobe (EMP) analysis of MI in enclaves from El Hoyazo dacite. Special attention has been paid to the EMP analytical methodology, in order to obtain reliable alkali concentrations and ASI values (Aluminum Saturation Index = mol. $Al_2O_3/[CaO+Na_2O+K_2O]$) in the hydrated silicate glasses (Morgan and London, 1996, 2005). The study is primarily aimed to ascertain the origin and mechanisms of entrapment of MI, but also to provide preliminary information on the origin of glass compositions and cause of chemical heterogeneity. This information will serve as a base for future studies on the mechanisms of crustal anatexis of El Hoyazo enclaves.

2. Geological setting

Metapelitic enclaves have been collected from El Hoyazo dacites in the NVP, Betic Cordilleras (Fig. 1). The Betics in southern Spain and the Rif of northern Morocco constitute the western termination of the Alpine orogen in the peri-Mediterranean domain (e.g. Andrieux et al., 1971). They have resulted from a complex and still debated geodynamic scenario, related to the convergence of the Iberian and African lithospheric plates during late Mesozoic to Tertiary times (Andrieux et al., 1971; Sanz de Galdeano, 1990; Vissers et al., 1995).

The volcanics of the NVP are scattered through an SW–NE trending belt c. 200 km long and 25 km wide, located along the southeastern coast of Spain (Fig. 1). They range in composition from basaltic andesites to rhyolites, shoshonites, lamproites and alkali basalts, with crystallization ages of ≈15 to 2 Ma (Benito et al., 1999; Turner et al., 1999; Cesare et al., 2003a; Duggen et al., 2005). Their origin is still debated, in connection with the complex geodynamic scenario of the orogen. Different hypotheses involve diverse mantle reservoirs and variable degrees of interaction between mantle-

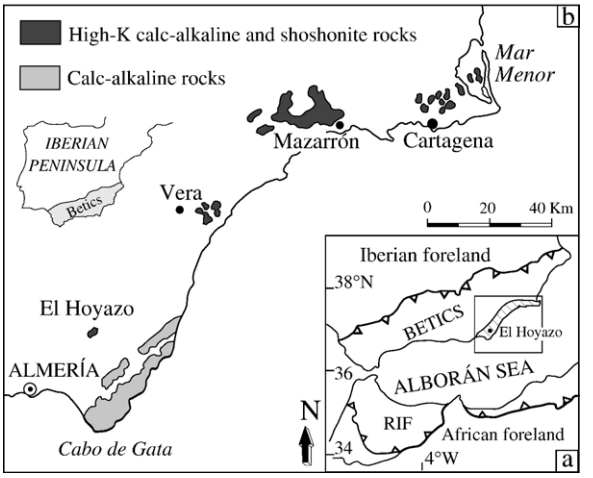

Fig. 1. Geographic location of (a) the Betic Cordilleras and Rif, and (b) volcanics of the Neogene Volcanic Province of southeastern Spain (after López Ruiz and Rodríguez Badiola, 1980).

derived melts and continental crust (e.g. Fernández-Soler, 1996; Benito et al., 1999; Turner et al., 1999; Duggen et al., 2005). El Hoyazo volcanic center is located SW in the volcanic belt, has a diameter of 1 km, consists of a pipe and surrounding block lava, is composed of dacites with ASI values as high as 1.5, and contains frequent enclaves (≈1–2 vol.%) of mainly metapelites and gabbros/basalts (Munksgaard, 1984; Zeck, 1992; Benito et al., 1999). Metapelitic enclaves represent fragments of middle-to-lower continental crust, partially melted at ~800–850 °C and 5–7 kbar, depleted in a granitic melt component, and brought to surface within the host dacites ≈6 Ma ago (Zeck, 1968, 1970; Munksgaard, 1984; Cesare et al., 1997, 2003a). These rocks have been interpreted as restites by most authors on the basis of petrography and geochemistry (i.e. El Hoyazo dacite derives largely from the partial melting of a metasedimentary protolith whose residue after melt extraction is represented by the crustal enclaves; Zeck, 1968, 1970; Munksgaard, 1984; Cesare et al., 1997; Benito et al., 1999).

Cesare and coworkers have used a variety of techniques in their studies on El Hoyazo enclaves to gain information on the process of crustal anatexis in this particular natural case (e.g. Cesare et al., 1997, 2003a,b, 2006—this issue). The main stage of anatexis currently recognizable in the rocks took place at 850±50 °C and 5–7 kbar. Some enclaves show, however, well developed quartz-absent biotite melting reactions, indicating a further stage of melting at 900–950 °C and ≈5 kbar. Hence melt in the enclaves seems to have formed over a temperature interval of ≈50–150 °C. Partial melting was H_2O-undersaturated, although a C–O–H fluid was present at some point during anatexis. The 850±50 °C anatectic event occurred during deformation and development of a foliation and, therefore, melting took place on a regional scale and before incorporation of enclaves into the dacite. About 30–60 wt.% of melt has been extracted from the protolith, leading to the restitic character of enclaves. Melt loss at the scale of hand specimen was due to flow along foliation planes during ductile deformation. Nominally all mineral phases in the enclaves crystallized (or recrystallized) in the presence of melt. Because no melting reaction is known that generates as peritectic plates all restitic minerals present in the rock, it was proposed that melting was produced by the very rapid heating of a phyllite, transforming the low-grade assemblage directly into the anatectic assemblage and by-passing intermediate reactions and stages of equilibrium. The geodynamic scenario associated with anatexis consists of partial melting at or near the base of a thinned continental crust in contact with hot asthenospheric mantle or basalts, during extension of the Betic Cordilleras.

3. Petrography

Previous studies have classified metapelitic enclaves at El Hoyazo into two main petrographic types, Grt–Bt–Sil and Spl–Crd (Zeck, 1968, 1970; Cesare et al., 1997). The current study deals only with MI within minerals of Grt–Bt–Sil enclaves, which are characterized by a quartz-absent assemblage consisting of variable modal proportions of plagioclase, biotite, sillimanite, garnet, cordierite, ilmenite, graphite and matrix glass, with rare alkali feldspar. Cesare et al. (2005) have further divided the Grt–Bt–Sil type into Bt-rich and Bt-poor samples, inferred to be genetically related by progressive dehydration melting of Bt (see also Benito et al., 1999). Biotite-rich enclaves are characterized by the abundance of plagioclase, scarcity or absence of cordierite, and high Bt/Crd modal ratios (e.g. see Fig. 2 of Cesare et al., 1997). Matrix glass is present as hundreds of μm- to mm-thick films parallel to foliation and pods in contact with all major mineral phases. Matrix glass may appear partially crystallized (up to ≈50% in volume) to skeletal-to-prismatic crystallites of alkali feldspars. Restitic feldspars in contact with matrix glass commonly show a 50–100 μm thick fringe, made of skeletal alkali feldspar, likely produced upon quenching. Fluid inclusions are absent in most samples, and MI are concentrated in plagioclase, garnet, and biotite. Biotite-poor enclaves are characterized by abundant cordierite, low Bt/Crd modal ratios and lower amount of plagioclase which, unlike in the Bt-rich subtype, shows strong optical zoning (see Fig. 1 of Cesare et al., 2005). Fluid inclusions are frequent; MI are much less abundant than in Bt-rich enclaves and appear mostly within plagioclase and cordierite. Matrix glass is scarce or absent.

4. Samples and methods

The microstructural relations of MI to their hosts have been studied in a variety of Grt–Bt–Sil enclaves, and the chemistry of glasses have been analyzed in inclusions within plagioclase, garnet, cordierite and ilmenite from five samples: Bt-rich HO-33, HO-50, and PFHZ-3; Bt-poor AVHZ-8; and sample AVHZ-7 bearing features intermediate between both sub-types.

Microstructures of enclaves were studied using optical microscopy and a CamScan MX2500 scanning electron microscope (SEM) at the Dipartimento di Mineralogia e Petrologia, Universitá di Padova. Glass within MI was

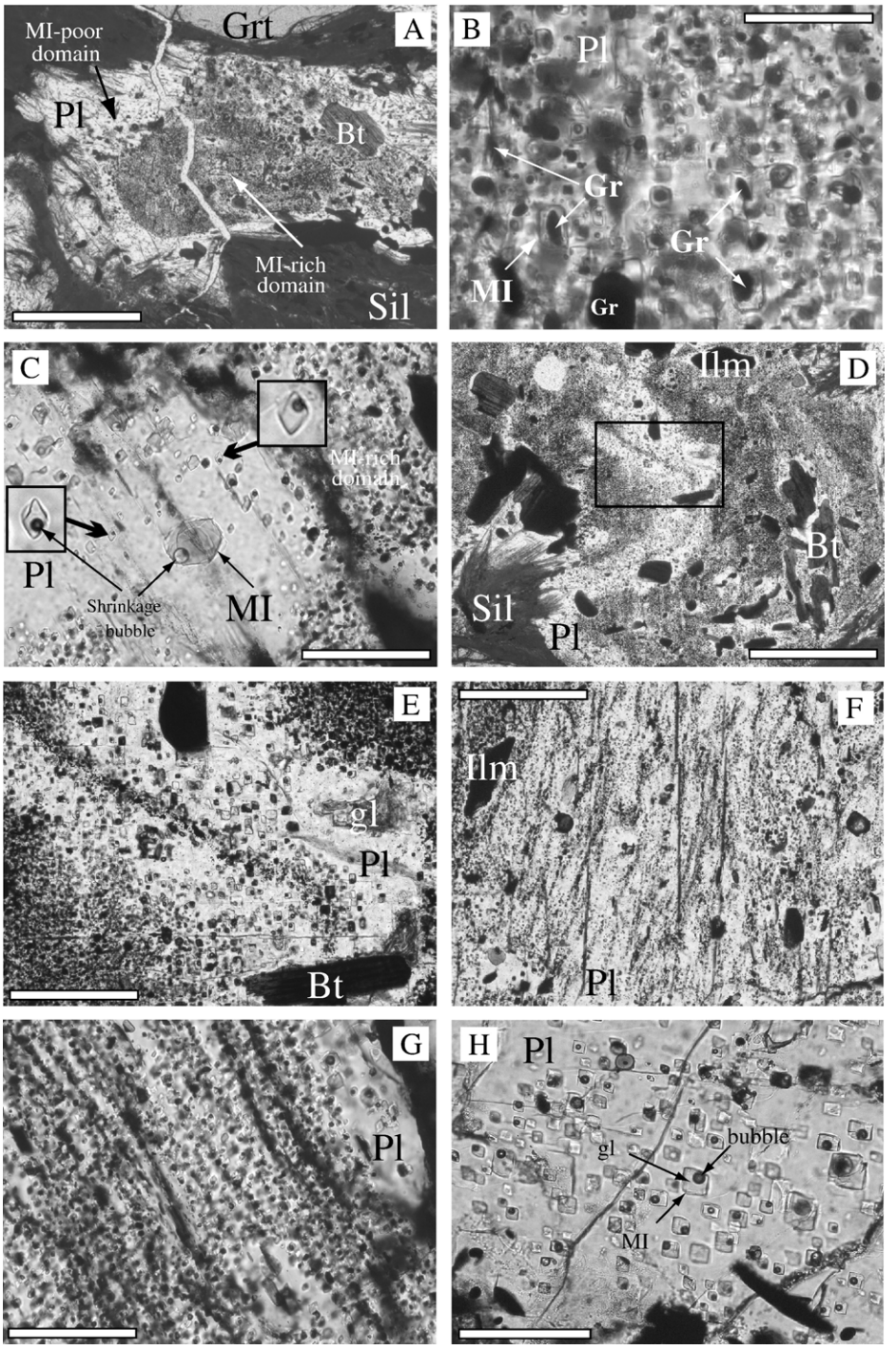

Fig. 2. Microstructures of MI in plagioclase of Bt-rich enclaves under optical microscope, plane polarized light (PPL). (A) Plagioclase crystal crowded with MI at the core and having scarce MI at the rim; scale bar ≈ 1 mm. (B) Detail of the core of former plagioclase. Many MI include graphite; scale bar ≈ 50 μm. (C) Plagioclase with heterogeneous distribution of MI: they are small and abundant in domains crowded with inclusions of graphite (upper right corner), and larger and scarce in domains free of mineral inclusions (center and left). Note sigmoidal shapes of some MI; scale bar ≈ 100 μm. (D) Plagioclase crystal with inclusions of mostly graphite and melt, delineating a micro-fold; scale bar ≈ 1 mm. (E) Detail of the hinge of previous micro-fold. Note the heterogeneous distribution of MI, and their undeformed negative crystal shape; scale bar ≈ 250 μm. (F) Graphite and MI within plagioclase aligned following a S–C type microstructure; scale bar ≈ 250 μm. (G) Foliation within plagioclase delineated by graphite and MI; scale bar ≈ 125 μm. (H) Most MI within plagioclase have negative crystal shape and are composed of undevitrified glass and a shrinkage bubble; scale bar ≈ 125 μm.

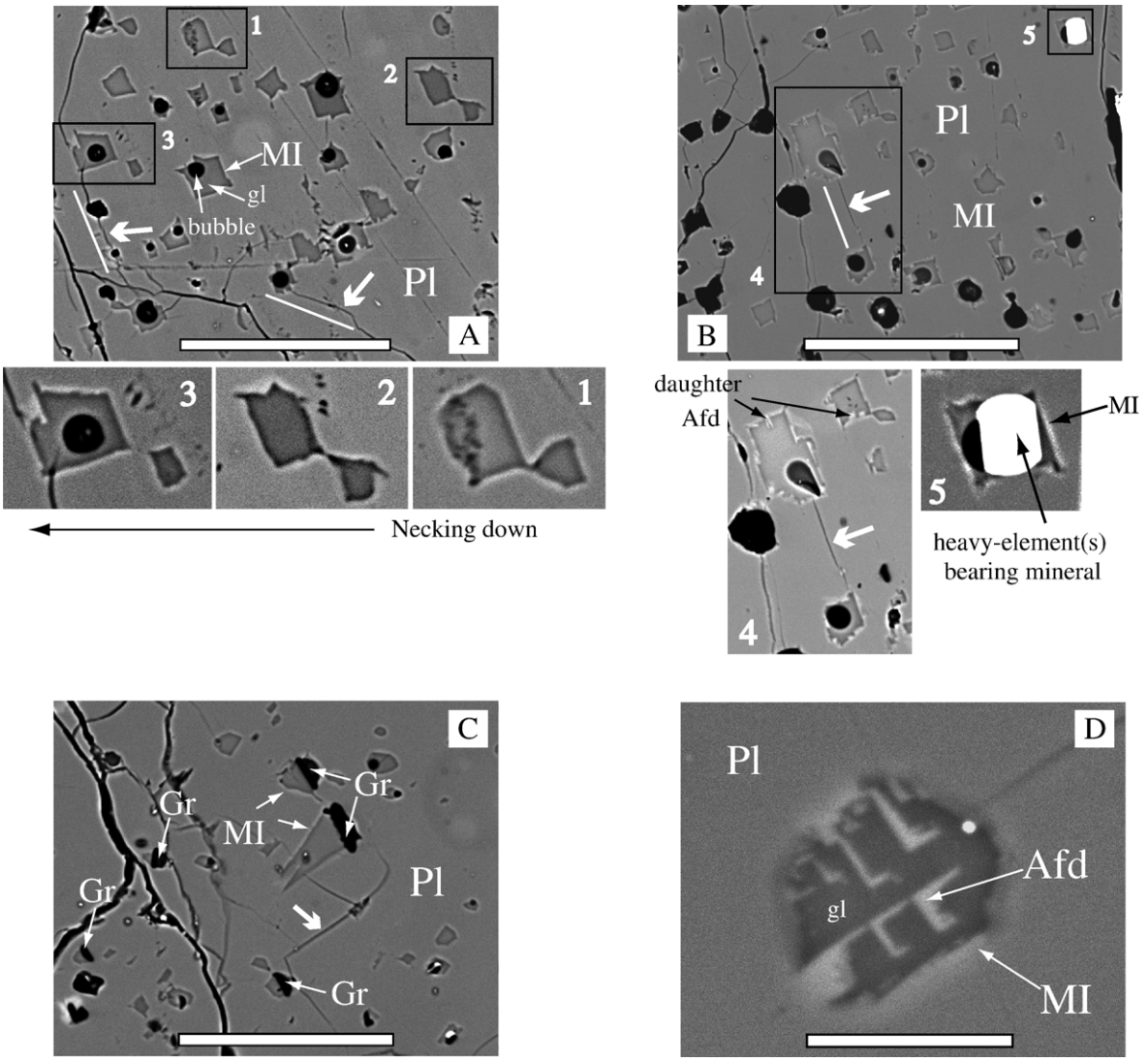

Fig. 3. Microstructures of MI in plagioclase of Bt-rich enclaves under scanning electron microscope (BSE images). (A, B) Melt inclusions mostly with negative crystal shape; some of them show necking down microstructures. Note planar structures filled with glass connecting MI (bold arrows, orientation marked by white lines); some of them parallel the orientation of MI with negative crystal shape. Often MI show daughter alkali feldspars nucleated on the walls (light crystals). Scale bars are ≈110 μm in (A) and ≈150 μm in (B). (C) Composite MI with graphite; graphite grains likely favored entrapment by ''poisoning'' plagioclase growth surfaces. Note planar structures filled with glass (bold arrow); scale bar is ≈110 μm. (F) Detail of MI with daughter skeletal alkali feldspars nucleated on the walls; scale bar is ≈15 μm.

analyzed with Cameca SX-50 electron microprobes (EMP) at the University of Oklahoma and Universitá La Sapienza of Rome. Analyses were only conducted on previously back-scattered electron (BSE) imaged MI. To avoid or minimize alkali loss and changes in major elemental ratios, two analytical conditions were used as recommended by Morgan and London (1996, 2005). Sodium, K, Al and Si were analyzed first and concurrently using an accelerating voltage of 20 kV, 2 nA current, and a 5 μm beam diameter. The elements Fe, Mn, Mg, Ti, Ca, P, F and Cl were analyzed with a 20-kV, 20-nA, 5-μm beam. Counting times were 30 s on peak for all elements, yielding 3σ minimum detection limits of ≈0.02 wt.% for Na_2O, K_2O and Al_2O_3, and ≈0.05 wt.% for SiO_2. Matrix reduction used the PAP correction algorithm (Pouchou and Pichoir, 1985). Relative uncertainties based on counting statistics are in the range of 0.5–1.0% for Al_2O_3 and SiO_2, and 1.5–3.0% for Na_2O and K_2O. Analyses were corrected using hydrated haplogranite glass of known composition as secondary standard. The maximum uncertainty for reported ASI values is ±0.035, calculated by the propagation of errors. Water concentrations in glass were

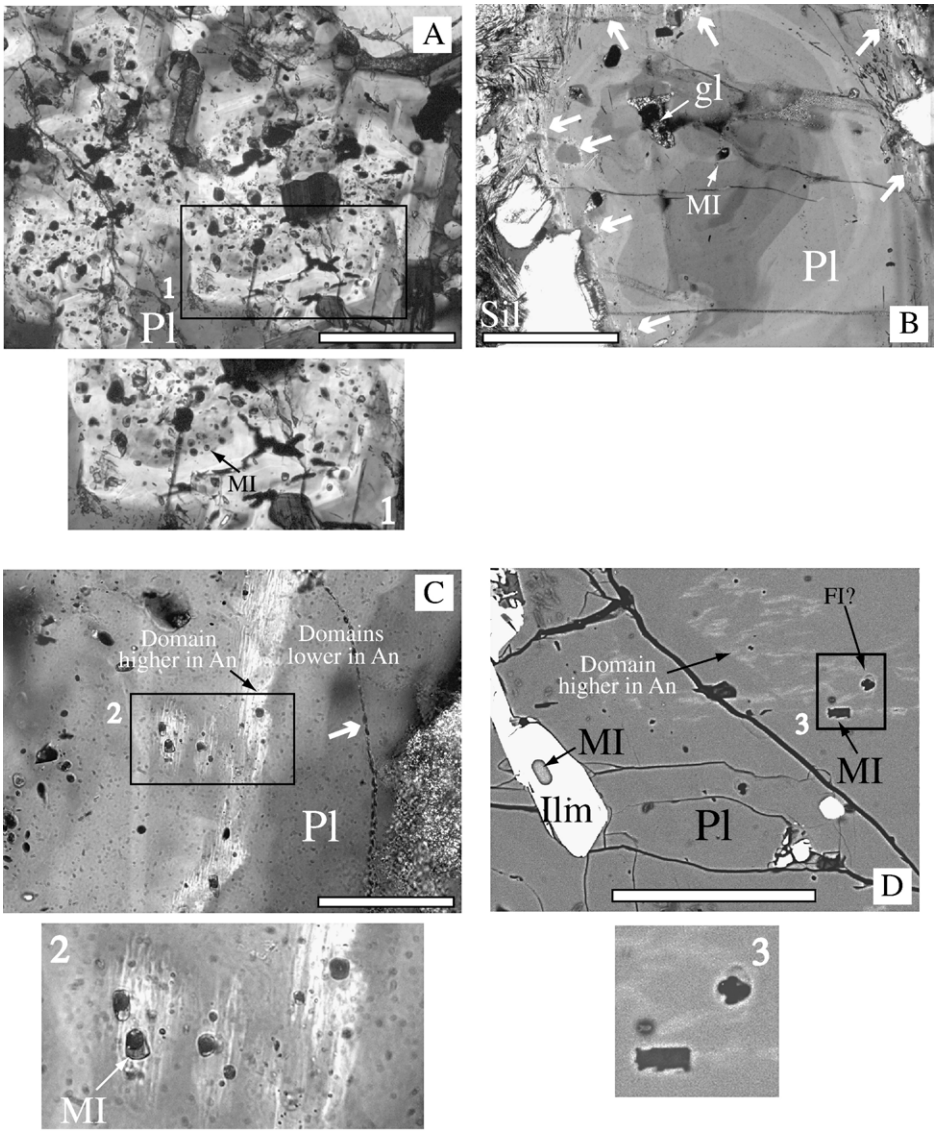

Fig. 4. Microstructures of MI within plagioclase of Bt-poor enclaves, under optical (crossed polars, XPL) (A–C) and scanning electron microscope (BSE image) (D). (A) Melt inclusions are concentrated at the core of crystal, and the boundary between MI-rich core and MI-poor rim follows optical zoning; scale bar is ≈250 μm. (B) Melt inclusions are concentrated within a rim-like irregular domain (bold arrows) at the edges of crystal (detail in C). A few large MI are also present at the core; scale bar is ≈500 μm. (C) Detail of rim of former plagioclase. Note the location of MI within irregular light (Ca-richer) domain. Bold arrow marks a trail of secondary inclusions; scale bar is ≈125 μm. (D) Rim of plagioclase showing MI located within irregular light domain; EDX analysis indicates that it corresponds to a plagioclase richer in Ca. Note fresh MI within ilmenite included in plagioclase; scale bar is ≈110 μm.

calculated by the difference of electron microprobe totals from 100%. Morgan and London (1996) and Acosta-Vigil et al. (2003) have shown that using the above analytical methods on granitic glasses, the accuracy of H_2O by difference is better than ±10% relative for H_2O concentrations in the range of 2–10 wt.%. This estimation might be slightly affected by the presence of trace elements in the glasses, as Cesare et al. (2003b) determined that their total concentration in MI within andalusite from comparable enclaves is ≈2500–5000 ppm.

5. Results

5.1. Microstructures of melt inclusions

5.1.1. Plagioclase

Plagioclase in Bt-rich enclaves is anhedral, variable in grain size (≈0.1–2 cm) and often elongated parallel to foliation in the rock when present. Plagioclase lacks optical zoning and is crowded with mineral inclusions (particularly graphite) and MI. The distribution of MI

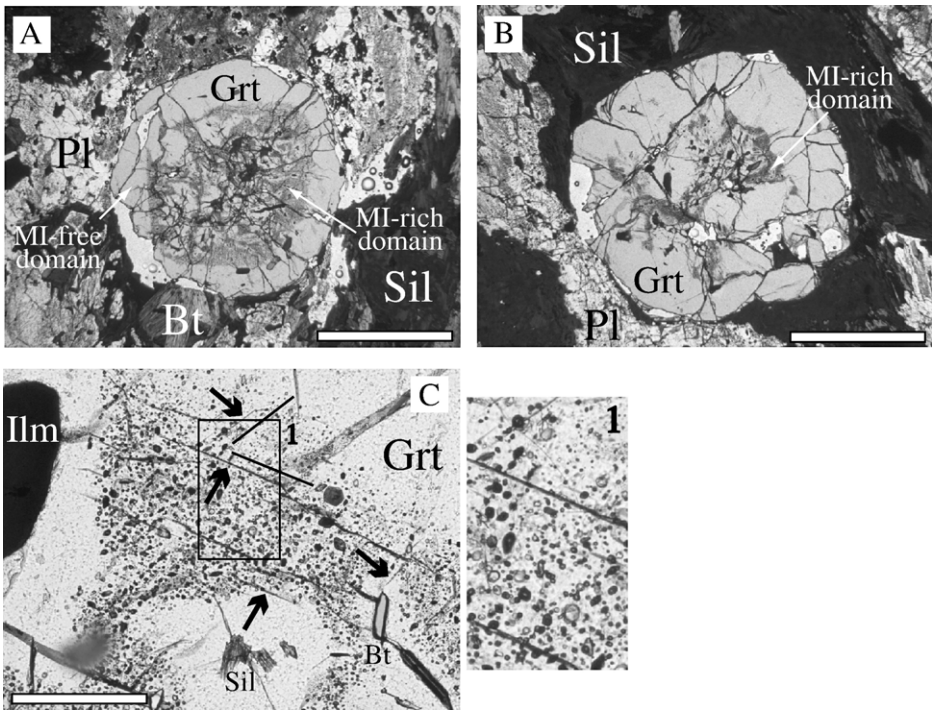

Fig. 5. Microstructures of MI within garnet of Bt-rich enclaves under optical microscope (PPL). (A, B) Melt inclusions are always located at the core of crystals. Boundaries between cores and MI-absent rims either mirror the crystallographic form of garnet (A) or are highly irregular (B); scale bar ≈ 2.5 mm. (C) Detail of garnet core crowded with MI. Note two sets of regularly-oriented planar discontinuities (arrows, orientation marked by black lines). The discontinuities do not extend into domains around large mineral inclusions; scale bar ≈ 250 μm.

within crystals is heterogeneous (Fig. 2A). Melt inclusions are numerous and small (≤ 10 μm) in regions of plagioclase crowded with small graphite inclusions, which generally corresponds to cores (Fig. 2A, B). Melt inclusions are larger (≈ 10–30 μm, sometimes up to 50–100 μm) and sparse in domains lacking small mineral inclusions (mostly at the rims) and in regions around large mineral inclusions (Fig. 2A, C). Melt inclusions appear either randomly orientated or arranged following either micro-folds (Fig. 2D, E), or S–C like microstructures (Fig. 2F), or a foliation (Fig. 2G) parallel both to the elongation of plagioclase grains and the foliation in the matrix. Most MI show negative crystal shape and are composed of clear undevitrified glass and a bubble (Fig. 2H). Raman spectroscopy indicated that bubbles are empty and represent shrinkage bubbles (Cesare and Maineri, 1999). Additionally, MI often include variable graphite in those plagioclase domains rich in melt and graphite inclusions (Fig. 2B). The variable glass/graphite ratios within MI indicate that graphite represents a solid inclusion and not a daughter mineral (see also Cesare and Maineri, 1999). Scanning electron microscope analysis reveals further information bearing on the mechanisms of entrapment and post-entrapment modifications of MI. Necking down phenomena are frequent (Fig. 3A). There are frequent linear (planar in 3D) discontinuities filled with glass that connect MI. Many of these planes are parallel to the orientation of MI with negative crystal shape and, therefore, likely have a crystallographic control (Fig. 3A, B). Most MI show daughter crystals of tabular or skeletal alkali feldspar nucleated on the walls (Fig. 3B, D).

Plagioclase of intermediate-type and Bt-poor enclaves has a grain size of 0.1–0.5 cm and show strong optical zoning. Compared with plagioclase of Bt-rich enclaves, mineral and melt inclusions are far less abundant; fluid inclusions, instead, are very abundant. The distribution of MI is controlled by the pattern of optical zoning. They concentrate either at the core (Fig. 4A) or within a rim-like irregular domain, richer in Ca, toward the edges (Fig. 4B–D). Melt and fluid may coexist within the same inclusion, and microstructures indicate entrapment of coexisting immiscible phases (see Cesare et al., 2006—this issue).

5.1.2. Garnet

Garnet of Bt-rich enclaves is subhedral and ≈ 0.1–0.5 cm in diameter. Melt inclusions within garnets are numerous, 5–10 μm in size with a few reaching 10–20 μm, and always located at the core of crystals and

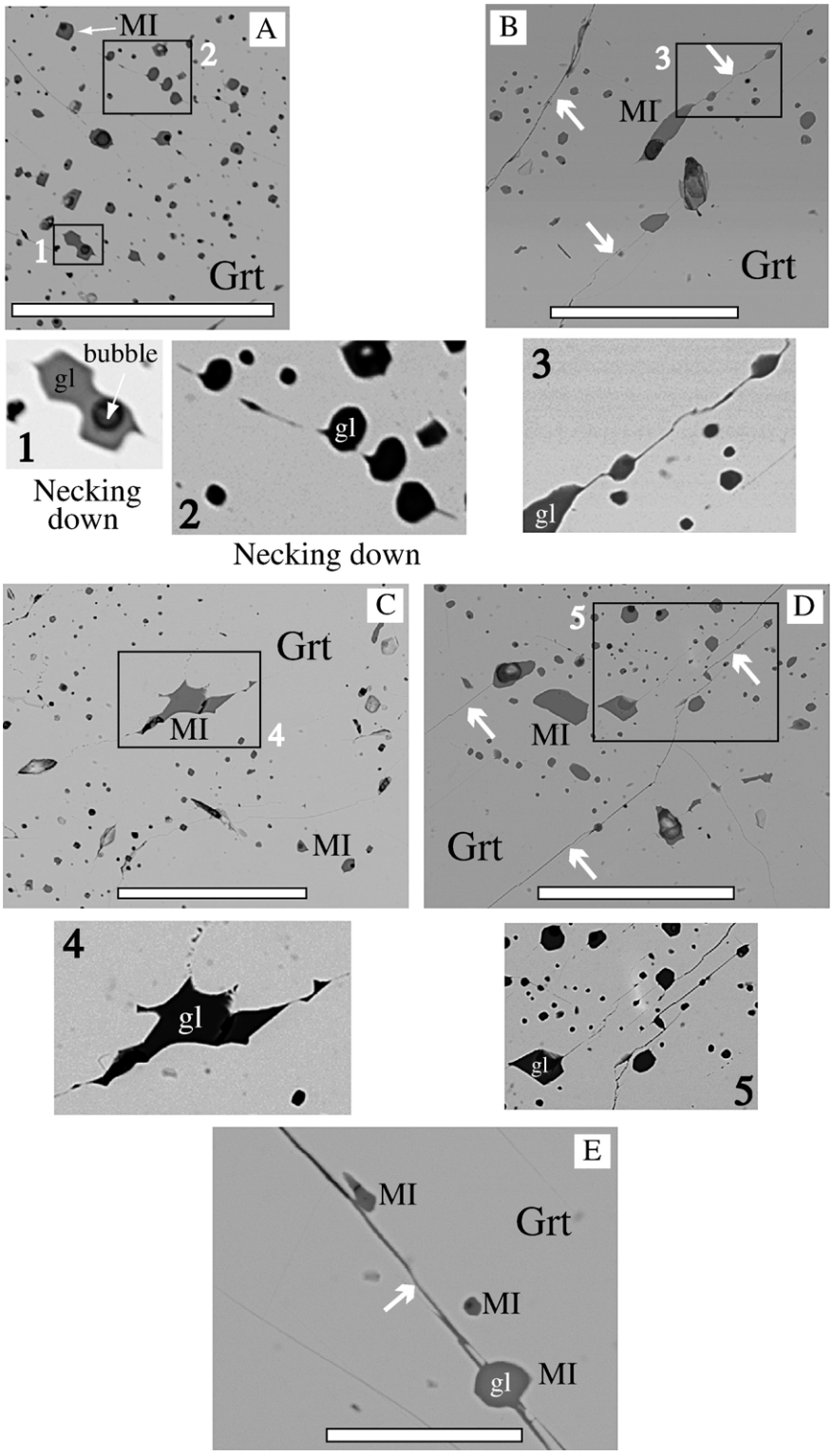

Fig. 6. Scanning electron microscope images (BSE) of MI within garnet of Bt-rich enclaves. (A) Melt inclusions showing necking down microstructures; scale bar ≈ 175 μm. (B–D) Melt inclusions with either negative crystal shape, or irregular shape and associated with planar discontinuities (marked by arrows) filled with glass; scale bars are ≈ 125 μm in (B), ≈ 160 μm in (C) and ≈ 150 μm in (D). (E) Detail of MI connected by planar discontinuity filled with glass; scale bar ≈ 35 μm.

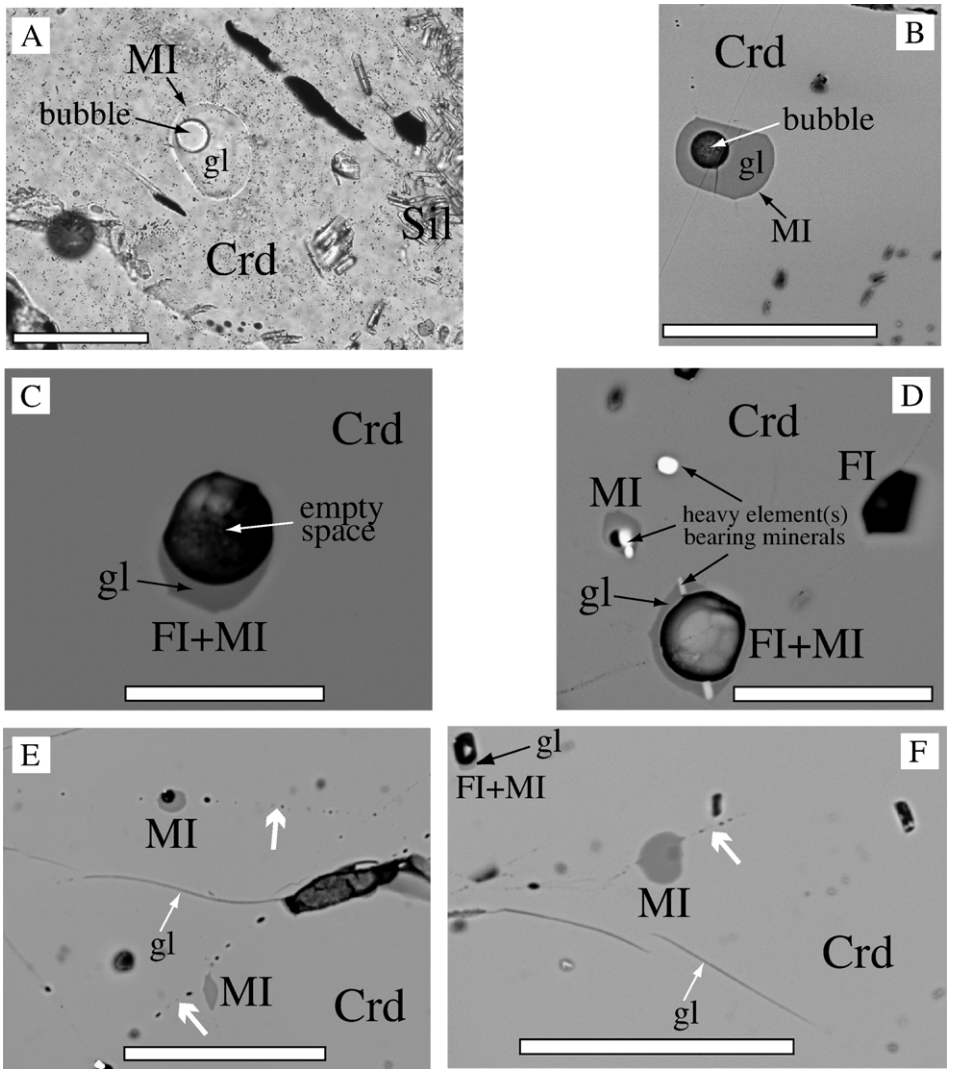

Fig. 7. Melt inclusions within cordierite of Bt-poor enclaves under optical microscope (PPL) (A) and SEM (BSE) (B–F). (A, B) Melt inclusions are made of fresh glass and shrinkage bubble; scale bars are ≈125 μm in (A) and ≈100 μm in (B). (C) Glass and likely former fluid (now empty space) coexisting within the same inclusion; scale bar ≈20 μm. (D) Composite MI, fluid inclusion, and likely mixed melt + fluid inclusion within cordierite. Note the presence of heavy-element(s) bearing minerals included in cordierite and within MI; scale bar ≈15 μm. (E, F) Melt inclusions connected to partially healed discontinuities (marked by arrows); scale bars ≈80 μm.

absent at the rims (≈ a few hundred μm from the edges). The distribution of MI through the cores is dense (except around large mineral inclusions) and may mirror the crystallographic form of the host (Fig. 5). Boundaries between cores and inclusion-free rims are sharp, though no compositional discontinuity has been observed under SEM. Regions of garnet with MI show two sets of linear discontinuities (likely planes in 3D), tens to hundred μm-long, intersecting at angles of ≈60° or 90° (Fig. 5C). Their nature is not clear as garnet does not present any cleavage, but the constancy in their relative orientations strongly suggests a crystallographic control. Melt inclusions usually form trends which parallel the discontinuities (Fig. 5C). Most MI show regular (cubic, dodecahedral) negative crystal shapes under optical microscope. However, BSE imaging reveals abundant necking down phenomena (Fig. 6A) and tube-like or irregular shapes (Fig. 6B, C). Glass may fill the planar, regularly-oriented discontinuities, which connect MI (Fig. 6B, D, E). Melt inclusions are composed of undevitrified glass, an empty shrinkage bubble (Fig. 6A) and, occasionally, include graphite or heavy element(s)-bearing minerals. Garnets in Bt-poor enclaves are MI-free in the studied samples.

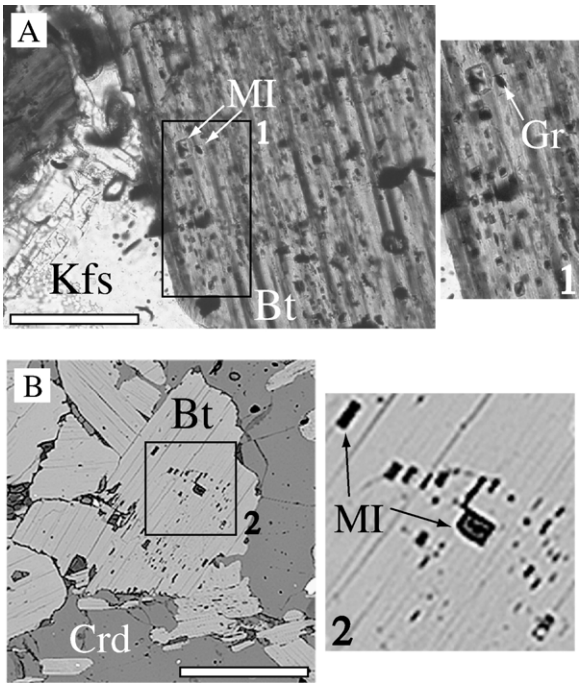

Fig. 8. Melt inclusions within biotite of Bt-rich enclaves, under optical microscope (A: scale bar ≈ 125 μm) and SEM (B: BSE, scale bar ≈ 400 μm).

5.1.3. Cordierite

Cordierite forms anhedral grains up to ≈ 1 cm in size and contains numerous mineral inclusions, mostly of biotite and fibrolite, which often define an internal foliation. Cordierites of Bt-rich enclaves are scarce and free of MI and FI. Cordierites of Bt-poor samples contain abundant FI and frequent MI. Melt inclusions have elliptical or spheroidal shape and are among the largest observed in the enclaves, with diameters of ≈ 10–100 μm and mean values of ≈ 20 μm (Fig. 7). They are mostly composed of clear undevitrified glass and an empty shrinkage bubble (Fig. 7A, B); rarely, they include sillimanite needles or heavy-element(s) bearing minerals (Fig. 7D). Glass and fluid may form mixed inclusions with microstructures indicative of immiscible trapping (Fig. 7C, D, F) (see also Cesare et al., 2006—this issue). Some MI are connected to partially healed planar discontinuities filled with melt or likely former fluid phase (now empty space) (Fig. 7E, F).

5.1.4. Biotite

Biotite within Bt-rich enclaves has a grain size of ≈ 0.2–1 mm and occurs: as subhedral inclusions in other major mineral phases; as decussate aggregates in the matrix; and as anhedral grains within fibrolite mats. Melt inclusions are frequent to abundant within all textural types of biotite. They show prismatic to squared negative crystal shape, have a size of 5–20 μm, are commonly oriented parallel to cleavage planes, and often include graphite grains (Fig. 8). EDX analysis indicates that glass in MI is altered. Biotite of Bt-poor enclaves is scarce and mostly anhedral. It occurs as individual grains within the matrix or included in plagioclase, garnet or, most commonly, cordierite. Melt inclusions are scarce.

5.1.5. Alkali feldspar

Although present in most Bt-rich enclaves, alkali feldspar is scarce. It occurs as anhedral grains ≈ 1–5 mm across, in places inter-grown with plagioclase. Melt inclusions are rare, isolated, ≈ 5–20 μm in diameter, with prismatic negative crystal shapes. They are composed of clear glass, an empty shrinkage bubble, and sometimes contain solid inclusions of graphite, which seems to have favored entrapment (Fig. 9). Alkali feldspar in Bt-poor enclaves is frequent and forms large anhedral (up to 4 mm) or small subhedral (< 1 mm) crystals. Melt inclusions have not been observed.

5.1.6. Accessory minerals

Ilmenite is frequent and mostly forms globular grains ≈ 0.2–1 mm in size, either in the rock matrix or included within most of the major mineral phases. Melt inclusions in ilmenite are frequent, rounded or elliptical in shape, and variable in size (Figs. 4D and 10). They are, though, among the largest MI observed within El Hoyazo enclaves, with sizes up to ≈ 50–100 μm (Fig. 10B, C). Daughter crystals of ilmenite have grown from the walls of the largest inclusions (Fig. 10B, C). Apatite forms rounded to prismatic grains ≈ 50–200 μm in size, and appears mostly included within cordierite; melt inclusions are frequent. Melt inclusions are also present within zircon and monazite (see Cesare et al., 2003a). Melt inclusions within apatite, zircon and monazite are too small to analyze by EMP.

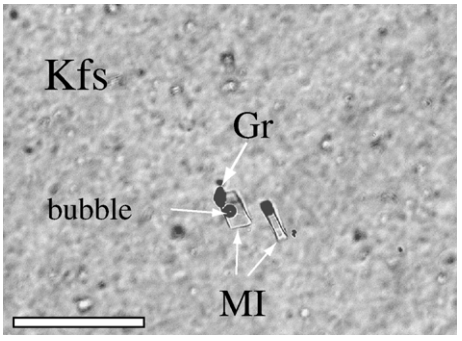

Fig. 9. Melt inclusions within alkali feldspar of Bt-rich enclaves under optical microscope; scale bar ≈ 90 μm.

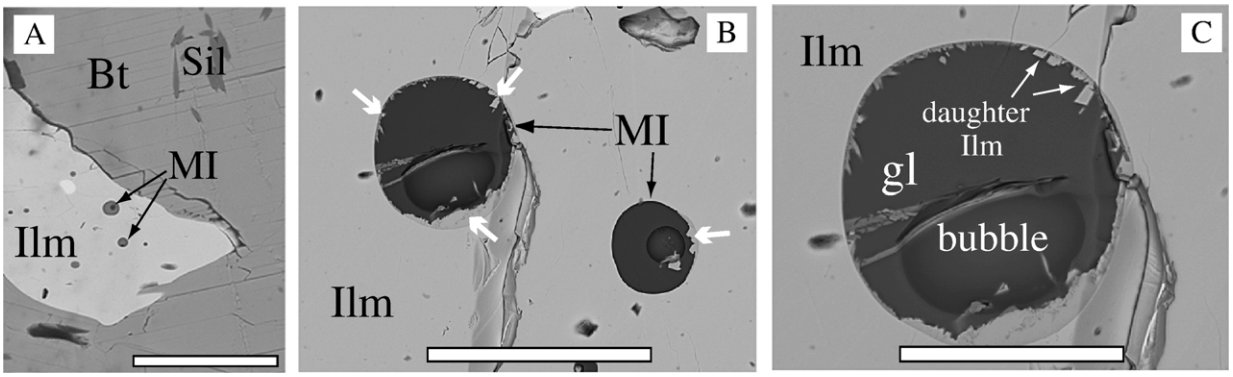

Fig. 10. Back scattered electron images of MI within ilmenite from Bt-poor enclaves (A: scale bar ≈ 85 μm; B: scale bar ≈ 140 μm). Note the crystallization of daughter ilmenite (bold arrows) within the largest MI. (C) is an enlargement of (B); scale bar ≈ 70 μm.

5.2. Melt inclusions major element compositions

Electron microprobe analyses from MI in plagioclase, garnet, cordierite and ilmenite have yielded granitic compositions (Table 1). All glasses show high concentrations of SiO_2 and K_2O, variable Al_2O_3 and P_2O_5, moderate to low FeO_t, CaO and Na_2O, and low TiO_2 and MgO. Water concentrations by difference, although variable, always indicate H_2O-undersaturated melts at the inferred pressures of melting. ASI values are, for the most part, moderate to low and comparable to those obtained in recent experiments investigating the solubility of excess alumina in granitic melts (Acosta-Vigil et al., 2003). Magnesium numbers are very low. Mean wt % normative compositions plot in the vicinity of the H_2O-undersaturated (a_{H_2O}=0.1–0.4) haplogranite eutectics (Fig. 11). In accordance with previous reconnaissance studies (Cesare et al., 1997; Cesare and Gómez-Pugnaire, 2001; Cesare et al., 2003b) we have found small though

Table 1
Mean electron microprobe analyses of MI within different mineral hosts

Mineral host	Plagioclase	Garnet	Cordierite	Ilmenite
No. analyses	199	63	56	18
SiO_2	73.28 (1.48)	71.26 (1.44)	73.42 (0.95)	70.68 (1.30)
TiO_2	0.08 (0.04)	0.10 (0.03)	0.07 (0.05)	0.31 (0.05)
Al_2O_3	12.64 (0.79)	14.44 (0.33)	14.01 (0.39)	15.69 (0.80)
FeO*	1.15 (0.33)	1.72 (0.51)	1.31 (0.16)	2.58 (0.19)
MnO	0.02 (0.03)	0.08 (0.05)	0.04 (0.04)	0.07 (0.05)
MgO	0.15 (0.05)	0.05 (0.04)	0.04 (0.06)	0.13 (0.04)
CaO	0.24 (0.23)	0.60 (0.10)	0.93 (0.15)	0.96 (0.13)
Na_2O	2.85 (0.46)	3.61 (0.42)	3.41 (0.39)	3.55 (0.15)
K_2O	5.00 (0.58)	4.97 (0.30)	4.92 (0.60)	4.92 (0.17)
P_2O_5	0.21 (0.10)	0.37 (0.09)	0.20 (0.17)	0.31 (0.10)
F	0.06 (0.06)	0.08 (0.07)	0.05 (0.06)	0.07 (0.10)
Cl	0.04 (0.09)	0.01 (0.01)	0.45 (0.08)	0.01 (0.00)
O=F	−0.02 (0.03)	−0.03 (0.03)	−0.02 (0.03)	−0.03 (0.04)
O=Cl	−0.01 (0.02)	0.00 (0.00)	−0.10 (0.02)	0.00 (0.00)
H_2O by diff	4.31 (1.03)	2.74 (1.61)	1.27 (0.95)	0.75 (0.76)
#Mg	0.18 (0.03)	0.04 (0.02)	0.04 (0.06)	0.08 (0.02)
ASI	1.21 (0.10)	1.17 (0.08)	1.11 (0.04)	1.22 (0.04)
Norm Qtz	39.32	31.75	33.78	29.86
Norm Ab	26.04	32.89	30.28	32.22
Norm Or	31.90	31.62	30.52	31.20
Norm An	0.00	0.60	3.47	2.94
Norm Crn	2.74	3.14	1.95	3.78

*Total Fe as FeO.
Numbers in parentheses refer to 1-sigma standard deviations.

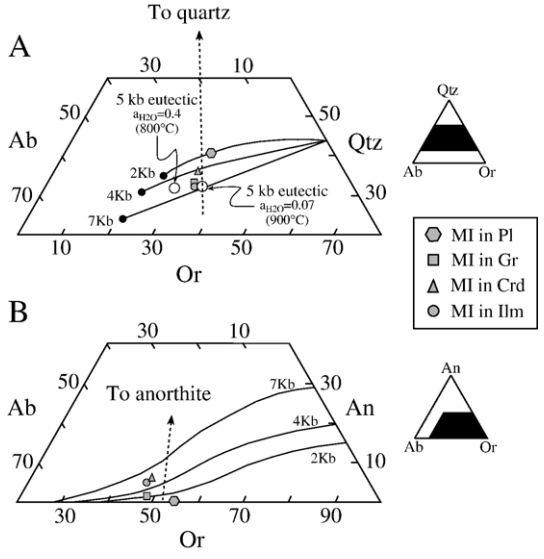

Fig. 11. Mean normative compositions (wt.%) of analyzed glasses within MI projected from An (A) or Qtz (B). The figure also shows haplogranite eutectic compositions at 2, 4 and 7 kbar and a_{H_2O}=1 (black circles) (taken from Winkler, 1974), and 5 kbar with a_{H_2O}=0.4 and 0.07 (open circles) (Ebadi and Johannes, 1991); and granite cotectic lines at 2, 4 and 7 kbar and a_{H_2O}=1 (Winkler, 1974).

systematic differences in glass composition among the several textural locations in the enclaves. Melt inclusions in plagioclase show the lowest Al_2O_3 and CaO concentrations, and highest MgO concentrations and #Mg values; MI in cordierite have the greatest CaO concentrations; MI in garnet show the highest FeO and P_2O_5 concentrations. Glass included in ilmenite is somewhat peculiar, with very high concentrations in Al_2O_3, FeO_t and TiO_2. In addition, we have also found a noticeable compositional variability of glass within each textural location (see standard deviations in Table 1, and Fig. 12). These characteristics are maintained among the several enclaves collected throughout the outcrop.

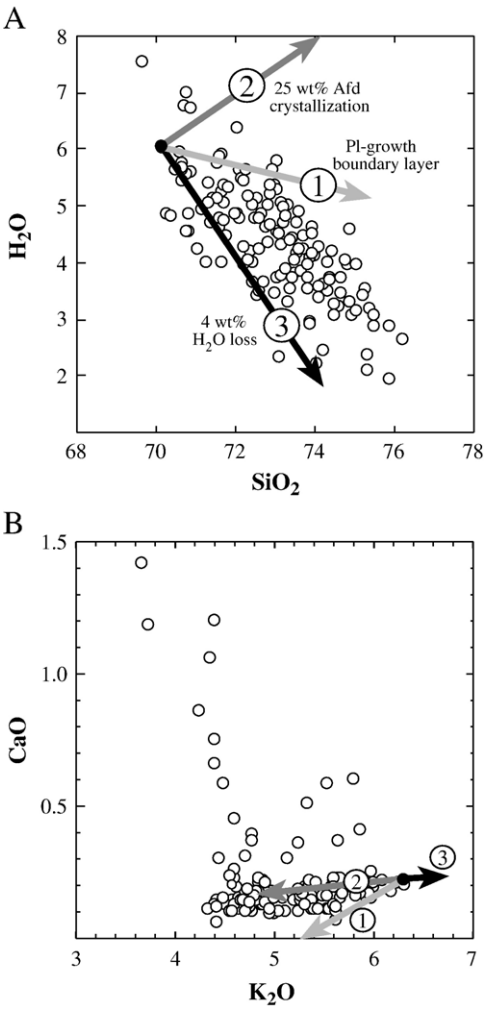

Fig. 12. Composition of MI analyzed within plagioclases of enclave HO-50. Arrows show the model compositional evolution of glasses due to (1) rapid plagioclase growth and creation of melt boundary layer, (2) crystallization of daughter Afd, and (3) loss of H by diffusion throughout plagioclase. Black circles represent the assumed starting composition for the modeling. See text for more explanation.

Moreover, glasses within a specific textural location have comparable compositions in the several enclaves that have been analyzed.

6. Discussion

6.1. Origin of melt inclusions and mechanisms of entrapment

Microstructures associated with MI in plagioclase of Bt-rich enclaves are complex and the following issues need explanation: (1) the heterogeneous distribution of MI at the scale of single grains; (2) the origin of MI alignments. The concentration of MI in domains rich in graphite, together with the occurrence of graphite both as mineral inclusions in plagioclase and within MI (Fig. 2), strongly suggests that: (1) the presence of small particles (mostly graphite) on the surface of growing crystals played an important role for entrapment of MI (Roedder, 1984) (see also Fig. 2 of Cesare et al., 1997, and Fig. 3 of Cesare and Maineri, 1999); (2) the previous matrix on which plagioclase have grown had an important role on the distribution of MI within this phase. Hence the heterogeneous distribution of MI can be explained by the effect of the matrix (and in particular graphite), together perhaps with variations in the rate of plagioclase growth: domains crowded with small MI (mostly cores) would have crystallized at a faster rate than domains with sparse and larger MI (mostly rims).

Alignments of MI may result from plagioclase crystallizing on a previously oriented matrix. For instance, Fig. 2D–E point to plagioclase growing on a foliated matrix affected by folding, with matrix minerals facilitating the entrapment of MI such that MI mimic previous folds. In some other cases alignments of MI may come from entrapment during crystal growth and deformation, as indicated by MI aligned parallel both to the elongation of plagioclase crystals and the foliation in the matrix, or by sigmoidal shapes of aligned MI (Fig. 2C) (see also Cesare et al., 1997; Cesare and Gómez-Pugnaire, 2001). The mostly dense distribution of MI within crystals and lack of continuity of alignments (e.g. at the rims of grains or around large mineral inclusions) argue against post-crystallization fracturing, percolation of melt, and later re-crystallization and necking down as responsible for alignments.

Backscattered electron images indicate that poisoning of crystal faces by small matrix minerals (e.g. graphite or heavy element(s)-bearing phases) was a common mechanism of MI entrapment. The presence of planar discontinuities filled with glass and connecting MI (Fig. 3A, B)

requires further explanation. Many MI show "tails" which parallel the orientation of some of these discontinuities (Fig. 3A), suggesting that MI likely represent the remains of former tabular volumes of melt after healing and necking down. Glass filling crystallographic-controlled discontinuities, such as those which parallel the orientation of MI with negative crystal shape (Fig. 3A–C), might represent (1) melt trapped on crystal faces during plagioclase growth (see Figs. 2–13 and 2–14 of Roedder, 1984), and/or (2) late fractures produced upon fast decompression following cleavage planes, that affected previously trapped MI, and along which the melt phase did percolate.

Microstructures indicate that entrapment of MI in plagioclase of Bt-poor enclaves was associated with: (1) the presence of particles on the surface of the growing plagioclase, e.g. MI with solid inclusions of graphite in Fig. 4A; (2) partial dissolution and later growth of plagioclase in the presence of melt, e.g. the large MI at the core of plagioclase in Fig. 4B, and MI located within the rim-like domain richer in Ca in Fig. 4B–D (see Roedder, 1984; compare also with plagioclase textures in Johannes, 1978, 1980). All the above observations and discussion strongly argue in favor of a primary origin for MI in plagioclase of Bt-rich and Bt-poor enclaves.

The distribution of MI within garnets of Bt-rich enclaves under optical microscope indicates a primary or pseudo-secondary origin (Fig. 5A). Planar discontinuities to which MI are associated (Figs. 5C and 6B, D, E) are interpreted either as former boundaries between adjacent garnet growth spirals, or crystallographic-controlled cracks produced in between garnet growth stages (see Fig. 2.21 of Roedder, 1984). Melt was trapped or percolated along these microstructures and, later on, necking down phenomena (Fig. 6A) individualized inclusions with negative crystal shape. We have found comparable major element compositions of glasses in MI with negative crystal shape and apparently unrelated to discontinuities, and in irregular MI connected to discontinuities. This suggests that all MI within garnet either have a similar origin or were trapped very close in time.

Microstructures of MI within cordierite, alkali feldspar and ilmenite are permissive of a primary origin: they are isolated, sparse, mostly unrelated to discontinuities and, in the case of cordierite and ilmenite, can be rather large (Figs. 7–10) (Roedder, 1984). However, some MI in cordierite are associated with partially healed planar discontinuities; moreover, planar discontinuities filled with glass are common (Fig. 7E, F). These are interpreted as late fractures produced upon fast decompression that intersected previously trapped MI. There are no differences among the major element compositions of isolated MI in cordierite (e.g. Fig. 7B) and those associated with partially healed discontinuities (e.g. Fig. 7E, F). Hence we conclude that most MI within cordierite are primary and/or pseudo-secondary and were trapped simultaneously or very close in time. Microstructures are also permissive of a primary or pseudo-secondary origin for MI in biotite (Fig. 8). However, alteration of most MI has occurred, likely due to chemical communication between MI and the rock matrix throughout cleavage planes.

6.2. Origin of melt inclusion compositions

The current study shows that microstructures associated with MI within El Hoyazo enclaves indicate in most cases a primary or pseudo-secondary origin of entrapment. All of the analyzed MI are composed of fresh undevitrified glass. Electron microprobe analyses of glasses have yielded peraluminous leucogranitic compositions (Table 1), and calculated H_2O concentrations are well below saturation values for granitic melts at the inferred pressures of melting (e.g. Holtz et al., 1995), strongly suggesting that crustal anatexis occurred under H_2O-undersaturated conditions. In fact, MI compositions are comparable to those of glasses produced by experimental fluid-absent partial melting of metapelites (e.g. Le Breton and Thompson, 1988; Vielzeuf and Holloway, 1988; Patiño Douce and Johnston, 1991). The presence of FI and MI in microstructures indicative of simultaneous entrapment of immiscible fluids and silicate liquid, however, testify for the coexistence of (CO_2-rich) fluid and melt, at least at some point during anatexis (see Cesare and Maineri, 1999; Cesare et al., 2006—this issue).

The most important addition of the current research program with respect to previous studies at El Hoyazo and most of the investigations dealing with MI in crustal environments, involves the novel and very large data set for the chemistry of MI in each of the textural locations of the rock (summarized in Table 1). This permits evaluating in detail the role of the several processes that may potentially control MI composition (Acosta-Vigil et al., in preparation), e.g. boundary layer phenomena, evolution along the liquid line-of-descent, dissolution of the host, crystallization of daughter minerals, and loss of H_2O by diffusion through the host (e.g. Roedder, 1984). A preliminary analysis of the chemistry of MI within plagioclases of HO-50 indicates that although none of the above processes can individually explain all features shown by glasses in variation diagrams, they likely have influenced melt compositions (Fig. 12). Loss of hydrogen via diffusion through host plagioclase may partially explain the conspicuous trend of decreasing H_2O with increasing SiO_2 (Fig. 12A); it does not explain, though,

either the entire SiO_2 concentration range (Fig. 12A) or trends shown by other oxides (Fig. 12B). The crystallization of daughter alkali feldspar is common and occurs to different degrees, hence it must partially account for variations in alkalis and CaO concentrations (Fig. 12B); it does not explain, however, trends shown by other oxides (Fig. 12A). The depletion of mineral components in melt adjacent to a growing crystal of plagioclase (generation of melt boundary layers) has been modeled using data on feldspar dissolution into peraluminous liquids from Acosta-Vigil et al. (2006b). This process should not be disregarded as it may partially account for the observed trends (Fig. 12), though in combination with other processes.

Despite the possible post-entrapment modifications, mean compositions of MI in the several textural locations can be tentatively interpreted as a record of the evolution of melt chemistry during prograde anatexis of quartz-poor metapelites. This interpretation is based on the following observations and assumptions. Previous studies have concluded that cordierite has crystallized late with respect to plagioclase, and that melt has been produced over a certain T interval (Cesare, 2000; Cesare et al., 2003a,b). The only major granitic component currently absent in the enclaves is quartz, whereas alkali feldspar is scarce and plagioclase is abundant. Mean compositions of MI approximately follow the tie-line joining quartz and glass compositions in pseudo-ternary Qtz–Ab–Or wt.% normative space (Fig. 11). Melt inclusions in plagioclase have the highest Qtz and lowest An normative compositions, and highest Or/Ab ratio, whereas MI in cordierite and ilmenite are lower in Qtz and show the highest An normative compositions and Ab/Or ratios.

7. Concluding remarks

This study provides the first extensive database on MI in natural samples of anatectic metapelites, through: (1) a very detailed microstructural study of MI in minerals of El Hoyazo enclaves, from which some of the mechanisms of entrapment can be deduced; (2) the characterization of MI compositions in several of the textural locations within the rock, with analyses conducted with the most appropriate EMP methodology in order to obtain reliable concentrations of alkalis and ASI values. Also, we report the likely evolution trend of melt composition during medium-to-low pressure prograde anatexis of quartz-poor graphite-saturated metapelites, though a more extensive study is needed to confirm this point (Acosta-Vigil et al., in preparation).

The example of anatexis at El Hoyazo represents an extremely relevant geologic site as it can provide information on the mechanisms of crustal melting in natural environments, e.g. the role of equilibrium melting versus the effect of kinetics on the composition of melt phase, or the extent to which granites image their protoliths. First, however, detailed experimental data on the following issues are needed for comparison: (1) the composition of melt phase during the prograde equilibrium melting of crustal protoliths, and in particular of quartz-poor pelites; (2) the kinetics of melting of crustal rocks.

Acknowledgements

Financial support for this work has been provided by the Italian Consiglio Nazionale delle Ricerche and the 01-LECEMA22F "WESTMED — Imaging the western Mediterranean margins: a key target to understand the interaction between deep and shallow processes" Project by the European Science Foundation under the EUROCORES Programme EUROMARGINS, through contract No. ERAS-CT-2003-980409 of the European Commission, DG. The Electron Microprobe Laboratory at the University of Oklahoma was created with US DOE grant DE-FG22-87FE1146 and upgraded with NSF grant EAR-9404658 and support from the University of Oklahoma Office of Research Administration. We thank C. Maineri and M.T. Gómez-Pugnaire for discussion, A. Álvarez-Valero for providing rock samples, M. Serracino for assistance with microprobe analyses, and Dima Kamenetsky and Csaba Szabó for thoughtful and constructive reviews that improved the original manuscript.

References

Acosta-Vigil, A., London, D., Morgan VI, G.B., Dewers, T.A., 2003. Solubility of excess alumina in hydrous granitic melts in equilibrium with peraluminous minerals at 700–800 °C and 200 MPa, and applications of the aluminum saturation index. Contrib. Mineral. Petrol. 146, 100–119.

Acosta-Vigil, A., London, D., Morgan VI, G.B., 2006a. Experiments on the kinetics of partial melting of a leucogranite at 200 MPa H_2O- and 690–800 °C: compositional variability of melts during the onset of H_2O-saturated crustal anatexis. Contrib. Mineral. Petrol. 151, 539–557.

Acosta-Vigil, A., London, D., Morgan VI, G.B., Dewers, T.A., 2006b. Dissolution of quartz, albite, and orthoclase in H_2O-saturated haplogranitic melt at 800 °C and 200 MPa: diffusive transport properties of granitic melts at crustal anatectic conditions. J. Petrol. 47, 231–254.

Alvarez-Valero, A., Cesare, B., Kriegsman, L.M., 2005. Formation of elliptical garnet in a metapelitic enclave by melt-assisted dissolution and reprecipitation. J. Metamorp. Geol. 23, 65–74.

Andrieux, J., Fontbote, J.M., Mattauer, M., 1971. Sur un modele explicatif de L'Arc de Gibraltar. Earth Planet. Sci. Lett. 12, 191–198.

Audétat, A., Günther, D., Heinrich, C.A., 2000. Magmatic–hydrothermal evolution in a fractionating granite: a microchemical study of the Sn–W–F-mineralized Mole Granite (Australia). Geochim. Cosmochim. Acta 64, 3373–3393.

Benito, R., López-Ruiz, J., Cebriá, J.M., Hertogen, J., Doblas, M., Oyarzun, R., Demaiffe, D., 1999. Sr and O isotope constraints on source and crustal contamination in the high-K calc-alkaline and shoshonitic neogene volcanic rocks of SE Spain. Lithos 46, 773–802.

Braun, I., Kriegsman, L.M., 2001. Partial melting in crustal xenoliths and anatectic migmatites: a comparison. Phys. Chem. Earth 26, 261–266.

Cesare, B., 2000. Incongruent melting of biotite to spinel in a quartz-free restite at El Joyazo (SE Spain): textures and reaction characterization. Contrib. Mineral. Petrol. 139, 273–284.

Cesare, B., Gómez-Pugnaire, M.T., 2001. Crustal melting in the Alborán domain: constraints from enclaves of the Neogene Volcanic Province. Phys. Chem. Earth 26, 255–260.

Cesare, B., Maineri, C., 1999. Fluid-present anatexis of metapelites at El Joyazo (SE Spain): constraints from Raman spectroscopy of graphite. Contrib. Mineral. Petrol. 135, 41–52.

Cesare, B., Salvioli Mariani, E., Venturelli, G., 1997. Crustal anatexis and melt extraction during deformation in the restitic xenoliths at El Joyazo (SE Spain). Min. Mag. 61, 15–27.

Cesare, B., Gómez-Pugnaire, M.T., Rubatto, D., 2003a. Residence time of S-type anatectic magmas beneath the Neogene Volcanic Province of SE Spain: a zircon and monazite SHRIMP study. Contrib. Mineral. Petrol. 146, 28–43.

Cesare, B., Marchesi, C., Hermann, J., Gomez-Pugnaire, M.T., 2003b. Primary melt inclusions in andalusite from anatectic graphitic metapelites: implications for the position of the Al_2SiO_5 triple point. Geology 31, 573–576.

Cesare, B., Meli, S., Nodari, L., Russo, U., 2005. Fe^{+3} reduction during biotite melting in graphite metapelites: another origin of CO_2 in granulites. Contrib. Mineral. Petrol. 149, 129–140.

Cesare, B., Maineri, C., Baron Toaldo, A., Pedron, D., Acosta-Vigil, A., 2006. Immiscibility between carbonic fluids and granitic melts during crustal anatexis: a fluid and melt inclusion study in the enclaves of the Neogene Volcanic Province of SE Spain. Chem. Geol. this issue.

Duggen, S., Hoernle, K., Van der Bogaard, P., Garbe-Schönberg, D., 2005. Post-collisional transition from subduction- to intraplate-type magmatism: evidence from continental-edge delamination of subcontinental lithosphere. J. Petrol. 46, 1155–1201.

Ebadi, A., Johannes, W., 1991. Beginning of melting and composition of first melts in the system Qz–Ab–Or–H_2O–CO_2. Contrib. Mineral. Petrol. 106, 286–295.

Fernández-Soler, J.M., 1996. El volcanismo calco-alcalino en el parque natural de Cabo de Gata-Níjar (Almería). Estudio volcanológico y petrológico. Sociedad Almeriense de Historia Natural. Monografías del Medio Natural, vol. 2, pp. 1–295.

Frezzotti, M.L., 2001. Silicate-melt inclusions in magmatic rocks: applications to petrology. Lithos 55, 273–299.

Frezzotti, M.L., Peccerillo, A., Zanon, V., Nikogosian, I., 2004. Silicate-rich melts in quartz xenoliths from Vulcano island and their bearing on processes of crustal anatexis and crust–magma interaction beneath the Aeolian arc, southern Italy. J. Petrol. 45, 3–26.

Grapes, R.H., 1986. Melting and thermal reconstitution of pelitic xenoliths, Wehr volcano, East Eifel, West Germany. J. Petrol. 27, 343–396.

Holtz, F., Behrens, H., Dingwell, D.B., Johannes, W., 1995. H_2O solubility in haplogranitic melts: compositional, pressure, and temperature dependence. Am. Mineral. 80, 94–108.

Johannes, W., 1978. Melting of plagioclase in the system Ab–An–H_2O and Qz–Ab–An–H_2O at P_{H_2O}=5 kbars, an equilibrium problem. Contrib. Mineral. Petrol. 66, 295–303.

Johannes, W., 1980. Metastable melting in the granite system Qz–Ab–Or–An–H_2O. Contrib. Mineral. Petrol. 84, 264–273.

Le Breton, N., Thompson, A.B., 1988. Fluid-absent (dehydration) melting of biotite in metapelites in the early stages of crustal anatexis. Contrib. Mineral. Petrol. 99, 226–237.

López Ruiz, J., Rodríguez Badiola, E., 1980. La región volcánica Neógena del sureste de España. Estud. Geol. 36, 5–63.

Lu, F., Anderson, A.T., Davis, A.M., 1992. Melt inclusions and crystal-liquid separation in rhyolitic magma of the Bishop Tuff. Contrib. Mineral. Petrol. 110, 113–120.

Morgan VI, G.B., London, D., 1996. Optimizing the electron microprobe analysis of hydrous alkali aluminosilicate glasses. Am. Mineral. 81, 1176–1185.

Morgan VI, G.B., London, D., 2005. The effect of current density on the electron microprobe analysis of alkali aluminosilicate glasses. Am. Mineral. 90, 1131–1138.

Munksgaard, N.C., 1984. High $\delta^{18}O$ and possible pre-eruptional Rb–Sr isochrons in cordierite-bearing Neogene volcanics from SE Spain. Contrib. Mineral. Petrol. 87, 351–358.

Patiño Douce, A.E., Johnston, A.D., 1991. Phase equilibria and melt productivity in the pelitic system: implications for the origin of peraluminous granitoids and aluminous granulites. Contrib. Mineral. Petrol. 107, 202–218.

Peppard, B.T., Steele, I.M., Davis, A.M., Wallace, P.J., Anderson, A.T., 2001. Zoned quartz phenocrysts from the rhyolitic Bishop Tuff. Am. Mineral. 86, 1034–1052.

Pouchou, J.L., Pichoir, F., 1985. "PAP" $\phi(\rho z)$ correction procedure for improved quantitative microanalysis. In: Armstrong, J.T. (Ed.), Microbeam Analysis. San Francisco Press, San Francisco, pp. 104–106.

Roedder, E., 1984. Fluid inclusions. Reviews in mineralogy. Am. Mineral. 12.

Salvioli-Mariani, E., Renzulli, A., Serri, G., Holm, P.M., Toscani, L., 2005. Glass-bearing crustal xenoliths (buchites) erupted during the recent activity of Stromboli (Aeolian Islands). Lithos 81, 255–277.

Sanz de Galdeano, C., 1990. Geologic evolution of the Betic Cordilleras in the Western Mediterranean, Miocene to the present. Tectonophysics 172, 107–119.

Thomas, R., Klemm, W., 1997. Microthermometric study of silicate melt inclusions in Variscan granites from SE Germany: volatile contents and entrapment conditions. J. Petrol. 38, 1753–1765.

Turner, S.P., Platt, J.P., George, R.M.M., Kelley, S.P., Pearson, D.G., Nowell, G.M., 1999. Magmatism associated with orogenic collapse of the Betic–Alborán domain, SE Spain. J. Petrol. 40, 1011–1036.

Vielzeuf, D., Holloway, J.R., 1988. Experimental determination of the fluid-absent melting relations in the pelitic system. Contrib. Mineral. Petrol. 98, 257–276.

Vissers, R.L.M., Platt, J.P., Van der Wal, D., 1995. Late orogenic extension of the Betic Cordillera and the Alborán Domain: a lithospheric view. Tectonics 14, 786–803.

Webster, J.D., Duffield, W.A., 1991. Volatiles and lithophile elements in Taylor Creek Rhyolite: constraints from glass inclusions analysis. Am. Mineral. 76, 1628–1645.

Webster, J.D., Thomas, R., Rhede, D., Förster, H.J., Seltmann, R., 1997. Melt inclusions in quartz from an evolved peraluminous pegmatite: geochemical evidence for strong tin enrichment in

fluorine-and phosphorus-rich residual liquids. Geochim. Cosmochim. Acta 61, 2589–2604.
Winkler, H.G.F., 1974. Petrogenesis of Metamorphic Rocks, third edition. Springer-Verlag, New York.
Zanon, V., Nikogosian, I., 2004. Evidence of crustal melting events below the island of Salina (Aeolian arc, southern Italy). Geol. Mag. 141, 525–540.
Zeck, H.P., 1968. Anatectic origin and further petrogenesis of almandine-bearing biotite–cordierite–labradorite dacite with many inclusions of restite and basaltoid material, Cerro de Hoyazo, SE Spain. PhD Thesis, Amsterdam.
Zeck, H.P., 1970. An erupted migmatite from Cerro de Hoyazo, SE Spain. Contrib. Mineral. Petrol. 26, 225–246.
Zeck, H.P., 1992. Restite–melt and mafic–felsic magma mixing and mingling in an S-type dacite, Cerro del Hoyazo, southeastern Spain. Trans. R. Soc. Edinb. Earth Sci. 83, 139–144.